Article

Structural, Electronic, and Magnetic Properties of Neutral Borometallic Molecular Wheel Clusters

Saira Perveen [ID] **and Nevill Gonzalez Szwacki** *[ID]

Faculty of Physics, University of Warsaw, Pasteura 5, PL-02093 Warsaw, Poland; sperveen@fuw.edu.pl
* Correspondence: gonz@fuw.edu.pl; Tel.: +48-22-55-32-797

Abstract: Atomic clusters exhibit properties that fall between those found for individual atoms and bulk solids. Small boron clusters exhibit planar and quasiplanar structures, which are novel materials envisioned to serve as a platform for designing nanodevices and materials with unique physical and chemical properties. Through past research advancements, experimentalists demonstrated the successful incorporation of transition metals within planar boron rings. In our study, we used first-principles calculations to examine the structure and properties of neutral boron clusters doped with transition metals, denoted as TMB_n and TMB_{2n}, where TM = Ti, Cr, Mn, Fe, Co, Nb, or Mo and $n = 8$–10. Our calculations show that the TMB_{2n} structures, which involve sandwiching metal atoms between two rings (called the drum configuration), and clusters with the single ring configuration, TMB_n, are stable. These clusters typically have relatively large HOMO-LUMO energy gaps, suggesting high kinetic stability and low chemical reactivity. Moreover, the clusters display interesting magnetic properties, determined not only by the metal atoms but also by the induced magnetism of the boron rings. These structures have potential applications in spintronics and sensing. This work also provides a basis for studying magnetism in the one-dimensional limit.

Keywords: borometallic clusters; planar boron clusters; first-principles calculations; nanostructure design

1. Introduction

Boron, a versatile element with applications spanning many fields, has a rich history that traces its origins to the isolation of simple boranes by Stock et al. [1]. Over the past two decades, a noteworthy chapter in this narrative has unfolded with the synthesis and characterization of various low-dimensional boron nanomaterials, including nanoclusters, nanowires, nanotubes, nanobelts, nanoribbons, and monolayer crystalline sheets [2–5]. Unlike traditional bulk boron crystals found in α-, β-, and γ-rhombohedral and α-tetragonal forms, these newly crafted boron-based nanomaterials have distinctive bonding patterns [6]. This departure gives rise to captivating physical and chemical properties, making them a focal point of fascination within materials science. Of particular note is the capability of boron-based nanomaterials, such as clusters, to serve as superatoms or as fundamental building blocks for crafting nanostructures designed with novel functionalities and properties. These systems are characterized by having diverse structures, including planar, quasiplanar, bowl, cage, tubular drum-like forms, multiple ring tubes, and fullerenes [7–11]. Electron deficiency of the boron atom enables its involvement in localized and delocalized bonding patterns across various geometric configurations. The neutral B_n clusters with $n < 20$ prefer a planar or quasiplanar structure [12]. On the other hand, B_n^- clusters retain

planarity (or quasiplanarity) for $n \leq 40$ [13]. The perfectly planar B_8 and B_9^- molecular wheels, with a hepta- or octacoordinated central boron atom, respectively, laid the foundation of borometallic clusters [14]. In the borometallic cluster, the central B atom is replaced by a metal atom, creating a similar doubly aromatic cluster [15,16]. Experiments in cluster beams have demonstrated that transition metal (TM) atoms can be incorporated into the center of the planar boron clusters [17–19].

In a more recent study by Zhang et al. [20], the CALYPSO structure search method was used to investigate the global minimum structures of neutral and negatively charged Ta_2B_n clusters, where n ranges from 1 to 10. Their findings revealed the formation of a B ring when n equals 6. Interestingly, the research identified a neutral Ta_2B_6 cluster exhibiting a bipyramidal configuration with enhanced stability. Chang Xu et al. [21] conducted a theoretical investigation on TM-centered double-ring clusters, $M@B_{2n}$ (where M = Ti, Cr, Fe, Ni, Zn and $n = 6, 7, 8$). They explored the factors contributing to the stability of these clusters in their study. Miao Yan et al. [22] introduced the concept of fluxional bonds in various structures, including planar B_{19}^-, tubular $Ta@B_{20}^-$, and cage-like B_{39}^-. These bonds form and break continuously on these systems' extremely flat potential energy surfaces. Ren et al. [23] used the CALYPSO method combined with density functional theory (DFT) calculations on niobium-doped boron clusters. Their research revealed that the global minima for the neutral clusters correspond to half-sandwich structures at $n = 10$–17 and tubular-type structures at $n = 18$–20. Chen et al.'s [24] study offered a comprehensive overview of the geometric configurations of both pure (B_n) and metal-doped boron clusters, which exhibit structures such as planar, nanotube, bilayer, fullerene-like, and core-shell forms across a wide range of cluster sizes (n). They also explored the potential for developing boron-based nanomaterials with specific functionalities derived from metal–boron clusters. Liu et al. [25] identified ten potential clusters made up of rings formed by 12 to 15 atoms of boron–carbon doped with heavier alkaline-earth (Ae) metals (Ae = Ca, Sr, Ba). Their chemical bond analysis reveals the important role of Ae d orbitals in facilitating covalent interactions between the central Ae atom and the surrounding boron–carbon rings.

Linear magnetic chains are becoming crucial in quantum information involving entanglement and correlation [26,27]. Carbon and boron-nitride-based nanotubes are used as support surfaces to stabilize unstable isolated atomic chains [28]. Photoelectron spectroscopy and theoretical studies identified metal-centered tubular ionic structures MnB_{16}^-, CoB_{16}^-, RhB_{18}^-, and TaB_{20}^- with a magnetic moment of 2, 2, 0, and 0 μ_B, respectively [29–32]. Neutral boron-based tubular structures, including FeB_{14}, FeB_{16}, UB_{20}, NpB_{20}, and PuB_{20}, were theoretically examined and found to have a quenched magnetic moment of $2\mu_B$ for the iron-based structures and relatively high magnetic moment of 3.69, 4.92, and 6.07 μ_B, respectively, for actinide-centered tubular structures [33,34]. These research works showed that the size and stability of the tubular structures greatly depend on the encapsulated metal atoms through the covalent bonds forming between the metal ions and the boron frame (MB_n) [35]. Metal-centered tubular boron clusters have been suggested as the building blocks for one-dimensional metallo-nanotubes [35]. However, the magnetic moments of TM-centered tubular boron clusters remain unexplored, with limited discussion on their magnetic behaviors.

In this work, using DFT calculations, we study the structure and properties of molecular borometallic wheel structures derived from planar boron B_8, B_9, and B_{10} wheel clusters. For all of these clusters, we analyze their magnetic behavior using spin-polarized calculations and analyze charge density differences and the contribution of metal and boron atoms to the density of states via the projected density of states (PDOS) analysis.

2. Computational Details

In our DFT-based study, we use the plane-wave-based Quantum ESPRESSO package [36]. The generalized gradient approximation (GGA) of Perdew–Burke–Ernzerhof (PBE) [37] is employed in the calculations combined with projector-augmented wave (PAW) pseudopotentials. Boron-based rings centered with TM atoms (TMB_n) are modeled by varying the value of n from 8 to 10 for single rings and subsequently increasing it to 16, 18, and 20 by taking the same ring twice and sandwiching the metal atom between them (TMB_{2n}). The TMB_n and TMB_{2n} clusters are shown in Figure 1. A vacuum distance of 16 Å is introduced to avoid interactions between cluster replicas. A plane-wave basis set with an energy cutoff of 70 Ry is used. The convergence threshold for the self-consistent energy calculations is 10^{-12}, and the atomic positions are optimized until the forces on atoms are smaller than 10^{-4} Ry/Bohr. The convergence threshold during phonon self-consistent calculations is 10^{-14} eV. All the computations are carried out at the Γ-point of the Brillouin zone. Assessing the stability of clusters often relies on the binding energy, E_b, as an important parameter. The calculation of E_b for the TMB_n and TMB_{2n} clusters is conducted using the following equation:

$$E_b = E(TMB_i) - E(B_i) - E(TM),$$

where $E(TMB_i)$ is the total energy of the optimized boron ring with the TM atom in the center, $E(B_i)$ is the total energy of the boron cluster in the ring ($i = n$) or drum ($i = 2n$) forms, and $E(TM)$ is the energy of the isolated TM atom. Spin-polarized calculations are carried out to study the magnetic properties of the clusters.
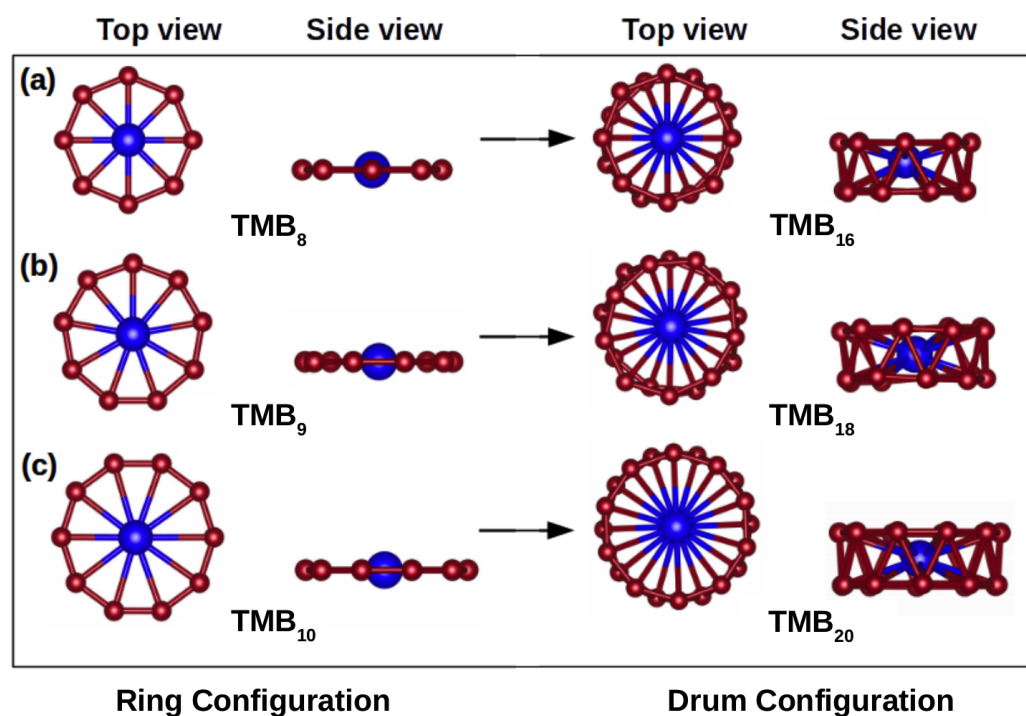
Figure 1. The structure of TMB_n (**left**) and TMB_{2n} (**right**) for $n = 8, 9,$ and 10 in (**a**–**c**), respectively. In each case, top and side views of the clusters are shown.

3. Results and Discussion

We became interested in the high symmetry of aromatic boron B_8 and B_9^- clusters, which are perfect heptagon and octagon structures with D_{7h} and D_{8h} symmetries, respectively [38]. This led us to conduct thorough investigations involving neutral clusters formed by replacing the central B atom in the octagon boron structure with TM counterparts, specif-

ically TM = Ti, Cr, Mn, Fe, Co, Nb, and Mo, and extending the study to larger borometallic clusters. Our investigation focused on two primary configurations: the above-mentioned "ring configuration" (TMB_n), featuring a TM atom at the center of a ring composed of 8, 9, or 10 boron atoms, and the "drum configuration" (TMB_{2n}), involving two rings of the same size stacked on top of each other, with the metal atom situated between the centers of two rings comprising 8, 9, or 10 boron atoms. Our system is visually represented in Figure 1, with boron atoms highlighted in dark red and forming a ring, and the central TM atom is shown in blue.

3.1. Structural Properties

In line with the structural arrangement shown in Figure 1, the bond lengths between adjacent boron atoms (d_{B-B}) and those connecting boron with central metal atoms (d_{B-TM}) are summarized for all the studied clusters in Table 1. It is worth noting that all the designed configurations are planar except for TiB_8, TiB_9, and FeB_8, where the central atom deviates slightly out of plane by 0.8387 Å, 0.6168 Å, and 0.8394 Å, respectively, giving rise to a distinctive bowl-like structure, which aligns well with previous research. The distances between metal and boron atoms (d_{B-TM}) for $n = 8, 9$, and 16 are small compared to their covalent bonds, indicating minimal steric repulsion between them. The bond length d_{B-B} is influenced by the number of B atoms present in the boron ring and the size of the central metal atom, especially for $n = 8$ and 9 (refer to Table 1). For TM = Cr, Mn, Fe, or Co, the drum configuration with the maximum number of boron atoms is only possible with B_{18} because, beyond that limit, an elliptical geometry prevails over a circular shape. In Table 1, we summarize the point group (PG) symmetry for each cluster, which was determined using the AFLOW software [39]. Except for the non-planar structures, the D_{4h} symmetry is assigned to TMB_8. For TMB_{10} clusters, the PG symmetry is D_{2h} due to its nearly circular geometry or C_{2h} due to its elliptical geometry. Similar trends have been reported for TaB_n^- clusters [40]: TaB_8^- forms a pyramidal structure, TaB_9^- shows increased planarity as the Ta atom integrates into a larger boron ring, and TaB_{10}^- achieves a perfectly planar, decacoordinated D_{10h} symmetry, representing the highest coordination for Ta in planar geometry, stabilized by aromaticity. Drum configurations mostly belong to the C_1 PG symmetry.

In Table 1, we have summarized the values of E_b for all the clusters. The E_b values consistently increase from TMB_8 to TMB_9 (or, in some cases, TMB_8 to TMB_{10}) and then decrease gradually until reaching TMB_{20} across all seven systems for each TM. Overall, the E_b values are relatively high for Co-doped configurations but notably lower for Mn-doped structures. It is important to note that all structures have negative E_b values, indicating the stability of the clusters since energy is required to separate them into TM and B_n.

3.2. Electronic Properties

In Table 1, we have summarized the HOMO-LUMO (H-L) energy gaps of the studied clusters. Although DFT-GGA underestimates energy gap values, most clusters still exhibit nonzero H-L energy gaps. The largest energy gaps for the ring configurations are found in CoB_9, NbB_{10}, and FeB_9, with values of 1.055 eV, 0.907 eV, and 0.785 eV, respectively. Among the drum configurations, the H-L energy gaps for MoB_{20}, CrB_{16}, and MnB_{16} (1.088 eV, 0.822 eV, and 0.804 eV, respectively) are larger compared to other drum structures. It is well established that DFT-based approaches systematically underestimate energy gaps [41]. Therefore, the true H-L energy gaps of the clusters may be even twice larger. Structures with large H-L energy gaps are associated with high kinetic stability and low chemical reactivity, making them promising candidates for future applications.

Table 1. Calculated parameters related to each studied structure: bond length between boron atoms (d_{B-B}), bond length between boron and metal atoms (d_{B-TM}), point group (PG), magnetic moment (m), H-L energy gap, and binding energy (E_b).

MB_n	d_{B-B} (Å)	d_{B-TM} (Å)	PG	m (μ_B)	H-L Gap (eV)	E_b (eV)
TiB_8	1.578	2.226	C_s	4	0.541	−9.667
TiB_9	1.558	2.335	C_s	3	0.090	−10.692
TiB_{10}	1.536	2.485	D_{2h}	2	0.617	−11.106
TiB_{16}	1.639	2.275	C_s	0	0.392	−8.214
TiB_{18}	1.608	2.460	C_1	2	0.246	−9.245
TiB_{20}	1.579	2.593	C_1	2	0.312	−7.925
CrB_8	1.587	2.073	D_{4h}	4	0.004	−11.476
CrB_9	1.551	2.269	C_s	3	0.367	−12.495
CrB_{10}	1.524	2.466	C_{2h}	2	0.357	−12.152
CrB_{16}	1.614	2.209	C_{2v}	0	0.822	−11.234
CrB_{18}	1.588	2.432	C_1	1.8	0.122	−10.471
CrB_{20}	1.608	2.645	C_1	4	0.425	−8.272
MnB_8	1.572	2.054	D_{4h}	3	0.486	−7.288
MnB_9	1.542	2.255	C_{2v}	2	0.880	−7.733
MnB_{10}	1.530	2.473	C_{2h}	3	0.264	−7.128
MnB_{16}	1.602	2.235	C_{2v}	1	0.804	−6.472
MnB_{18}	1.584	2.431	C_1	1	0.558	−5.397
MnB_{20}	1.602	2.723	C_1	3	0.439	−3.518
FeB_8	1.564	2.065	C_{4v}	2	0.016	−10.866
FeB_9	1.533	2.241	C_{2v}	1	0.785	−12.050
FeB_{10}	1.523	2.461	C_{2h}	2	0.274	−11.099
FeB_{16}	1.594	2.231	C_{4v}	1.49	0.063	−9.955
FeB_{18}	1.581	2.445	C_1	2	0.324	−8.645
FeB_{20}	1.617	2.760	C_1	2	0.268	−7.918
CoB_8	1.564	2.044	D_{4h}	1	0.001	−15.709
CoB_9	1.539	2.234	C_{2v}	0	1.055	−15.889
CoB_{10}	1.522	2.462	D_{2h}	3	0.404	−14.585
CoB_{16}	1.591	2.232	C_{4v}	1	0.297	−13.398
CoB_{18}	1.579	2.443	C_s	1	0.311	−11.828
CoB_{20}	1.619	2.749	C_1	1	0.258	−11.881
NbB_8	1.653	2.157	D_{4h}	3	0.504	−10.702
NbB_9	1.573	2.300	C_{2v}	2	0.418	−13.055
NbB_{10}	1.533	2.481	D_{2h}	1	0.907	−13.451
NbB_{16}	1.661	2.306	C_s	1	0.322	−10.318
NbB_{18}	1.561	2.477	C_1	1	0.362	−12.179
NbB_{20}	1.573	2.674	C_1	0	0.000	−10.937
MoB_8	1.628	2.126	D_{4h}	2	0.419	−12.395
MoB_9	1.560	2.281	C_{2v}	2.44	0.080	−14.021
MoB_{10}	1.524	2.467	C_s	0	0.092	−13.998
MoB_{16}	1.658	2.249	C_{2v}	0	0.616	−11.811
MoB_{18}	1.602	2.431	C_1	0	0.415	−12.663
MoB_{20}	1.568	2.760	C_1	0	1.088	−10.871

The PDOS spectra for all the clusters can be found in Section SI of the Supplementary Materials (SM). These spectra are valuable for studying the contribution of different atomic orbitals to the density of states in the studied clusters, particularly at and near the Fermi level, E_F. They also aid in visualizing the contribution of atomic orbitals to the magnetic properties of the clusters (e.g., to the shift between the spin-up and spin-down PDOS).

In general, the *p*-orbitals of boron and the *d*-orbitals of TMs make the most significant contributions to the density of states at the E_F. However, in specific cases such as TiB$_9$, FeB$_8$, CoB$_8$, and NbB$_{20}$, the contribution at the E_F comes solely from boron *p*-orbitals. A combination of boron *p* and TM *d* orbitals contribute to the density of states at the E_F for CrB$_8$, CrB$_{18}$, FeB$_{16}$, MoB$_9$, and MoB$_{10}$.

Cluster-specific observations, as inferred from the PDOS spectra, show distinct contributions to the highest occupied states, which can be summarized as follows: In the Ti series, B *p*-orbitals dominate in TiB$_9$, TiB$_{10}$, and TiB$_{20}$. In contrast, a mix of B *p* and TM *d* occurs in TiB$_8$, TiB$_{16}$, and TiB$_{18}$. In the Cr series, B *p*-orbitals significantly contribute in CrB$_9$ and CrB$_{16}$, and a mix of B *p* and TM *d* contributions occur in the rest of the Cr-based clusters. In the Mn and Fe series, the clusters frequently exhibit combined B *p* and TM *d* contributions with a consistent magnetic character. For Co-based clusters, the electronic configurations reveal that boron *p*-orbitals dominate the highest occupied states in CoB$_8$, CoB$_{16}$, CoB$_{18}$, and CoB$_{20}$, all of which are magnetic except for CoB$_8$, which lacks an H-L energy gap. In contrast, CoB$_9$ and CoB$_{10}$ exhibit contributions from both boron *p*- and TM *d*-orbitals to the highest occupied states, with CoB$_9$ being nonmagnetic and CoB$_{10}$ magnetic. Similarly, in Nb-based clusters, boron *p*-orbitals primarily contribute to the highest occupied states in NbB$_8$, NbB$_{16}$, and NbB$_{18}$, which are magnetic with H-L energy gaps, and NbB$_{20}$, which is nonmagnetic without an H-L energy gap. Clusters NbB$_9$ and NbB$_{10}$ exhibit combined contributions from boron *p*- and TM *d*-orbitals, maintaining magnetic properties and distinct H-L energy gaps. Finally, in the Mo series, most of the structures are nonmagnetic (e.g., MoB$_{18}$ and MoB$_{20}$), which is reflected in the symmetry of the spin-up and spin-down PDOS, contrasting with the magnetic nature of smaller clusters like MoB$_9$.

These observations highlight the nuanced role of TM *d*-orbitals and B *p*-orbitals in shaping the electronic and magnetic characteristics of borometallic clusters. The variability in orbital contributions underscores the tunable properties of these materials.

3.3. Vibrational Properties

The vibrational properties of the structures were analyzed using phonon computations to assess their stability. These calculations provide valuable insights into the dynamic behavior and structural integrity of the systems under study. According to the literature [42], a cluster is considered stable if all its real vibrational frequencies are positive and the minimum vibrational frequency, denoted as f_{min}, is significantly large. Table 2 presents the values of f_{min} for each cluster. For the ring configuration, TMB$_8$ and TMB$_9$ with TM = Ti, Cr, Mn, Fe, or Co have the highest values of f_{min}, whereas TMB$_9$ and TMB$_{10}$ clusters have the highest f_{min} for TM = Nb and Mo. Interestingly, the FeB$_{10}$ cluster in our calculations is at the border of stability as its f_{min} value is small but negative. For the drum configurations, there is less regularity, and large values of f_{min} are obtained for CrB$_{16}$, while the lowest value is for MnB$_{20}$. Our results for f_{min} are in close agreement with a study by Pu et al. [19], where the values of f_{min} for FeB$_9$ and CoB$_9$ were 110.5 cm^{-1} and 96.7 cm^{-1}, respectively. The complete list of phonon frequencies for each cluster is provided in Section SII of SM.

3.4. Dynamic Properties

To further verify the stability of the ring and drum structures, we performed quantum molecular dynamics (MD) simulations at two different temperatures with the choice of 1 fs for the time step. Each run was 3.5 ps long. At a temperature of 300 K, the ring and drum structures maintain their shape during the MD run, and no significant deformations occur. Both structure types deform at a temperature of 600 K but retain their wheel-like structure. This is shown in Figure 2 on the example of CoB$_9$ and MnB$_{18}$. It is worth noting that MnB$_{18}$ has one of the smallest E_b in absolute value.

Table 2. Minimum vibrational frequencies for each studied cluster.

Ring	f_{min} (cm^{-1})	Drum	f_{min} (cm^{-1})
TiB_8	206.22	TiB_{16}	48.41
TiB_9	123.91	TiB_{18}	65.62
TiB_{10}	85.00	TiB_{20}	78.17
CrB_8	87.93	CrB_{16}	160.53
CrB_9	196.47	CrB_{18}	59.27
CrB_{10}	44.03	CrB_{20}	89.9
MnB_8	140.21	MnB_{16}	122.13
MnB_9	135.68	MnB_{18}	130.70
MnB_{10}	69.60	MnB_{20}	27.00
FeB_8	133.40	FeB_{16}	75.14
FeB_9	128.48	FeB_{18}	79.27
FeB_{10}	−22.1	FeB_{20}	64.30
CoB_8	132.22	CoB_{16}	55.24
CoB_9	102.07	CoB_{18}	70.30
CoB_{10}	78.0	CoB_{20}	90.34
NbB_8	45.69	NbB_{16}	153.38
NbB_9	93.35	NbB_{18}	38.60
NbB_{10}	87.85	NbB_{20}	102.61
MoB_8	29.26	MoB_{16}	86.96
MoB_9	95.29	MoB_{18}	41.17
MoB_{10}	68.08	MoB_{20}	106.48
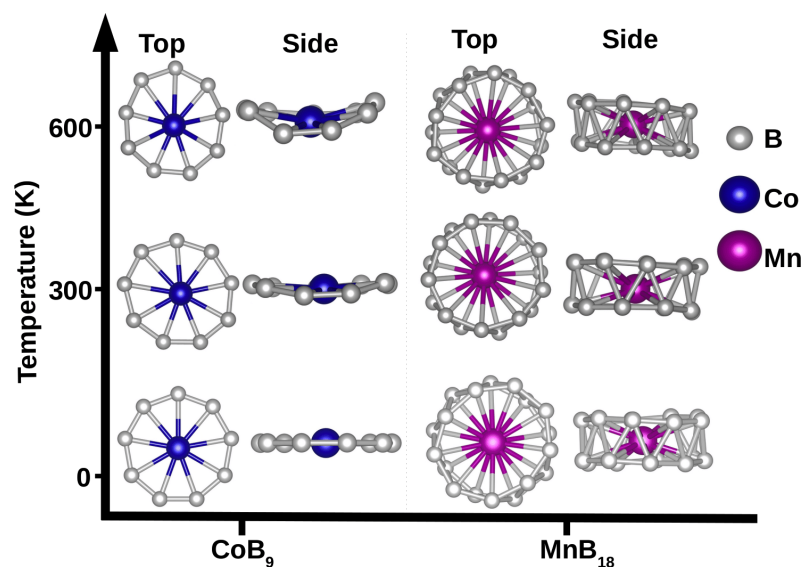
Figure 2. Ab initio molecular dynamics simulations at 300 K and 600 K. The top and side views of CoB_9 and MnB_{18} clusters are shown for each temperature.

3.5. Magnetic Properties

The magnetic moment values, denoted as *m*, for each cluster, are listed in Table 1. Generally, the value of *m* decreases as the number of boron atoms in the ring increases from 8 to 10. In contrast, an opposite trend is observed for drum structures, with *m* tending to increase as the number of boron atoms in the TMB$_n$ structure increases (from 16 to 20). Interestingly, the *m* values for CoB$_n$ and MoB$_n$ drum structures are independent of *n*, remaining equal to 1μ_B and 0μ_B, respectively.

The contribution from boron and TM atoms to magnetization is illustrated in Figure 3. In general, the contribution from TM atoms to total *m* is large. However, in most cases, the

boron atoms become polarized, resulting in a non-zero contribution to *m*. Specifically, for TMB$_8$ clusters, the boron contribution (represented by the yellow line) to *m* is consistently larger than the TM contribution (represented by the blue line). Conversely, metals demonstrate dominance in the case of TMB$_{10}$ structures. For drum configurations, both metal and boron atoms consistently exhibit positive (or zero) contributions to *m*, except for the case of Mn, where boron atoms have slightly negative local magnetization. The case of NbB$_n$ clusters is particularly interesting, as TM atoms induce the magnetization, but *m* is entirely localized on the boron atoms.
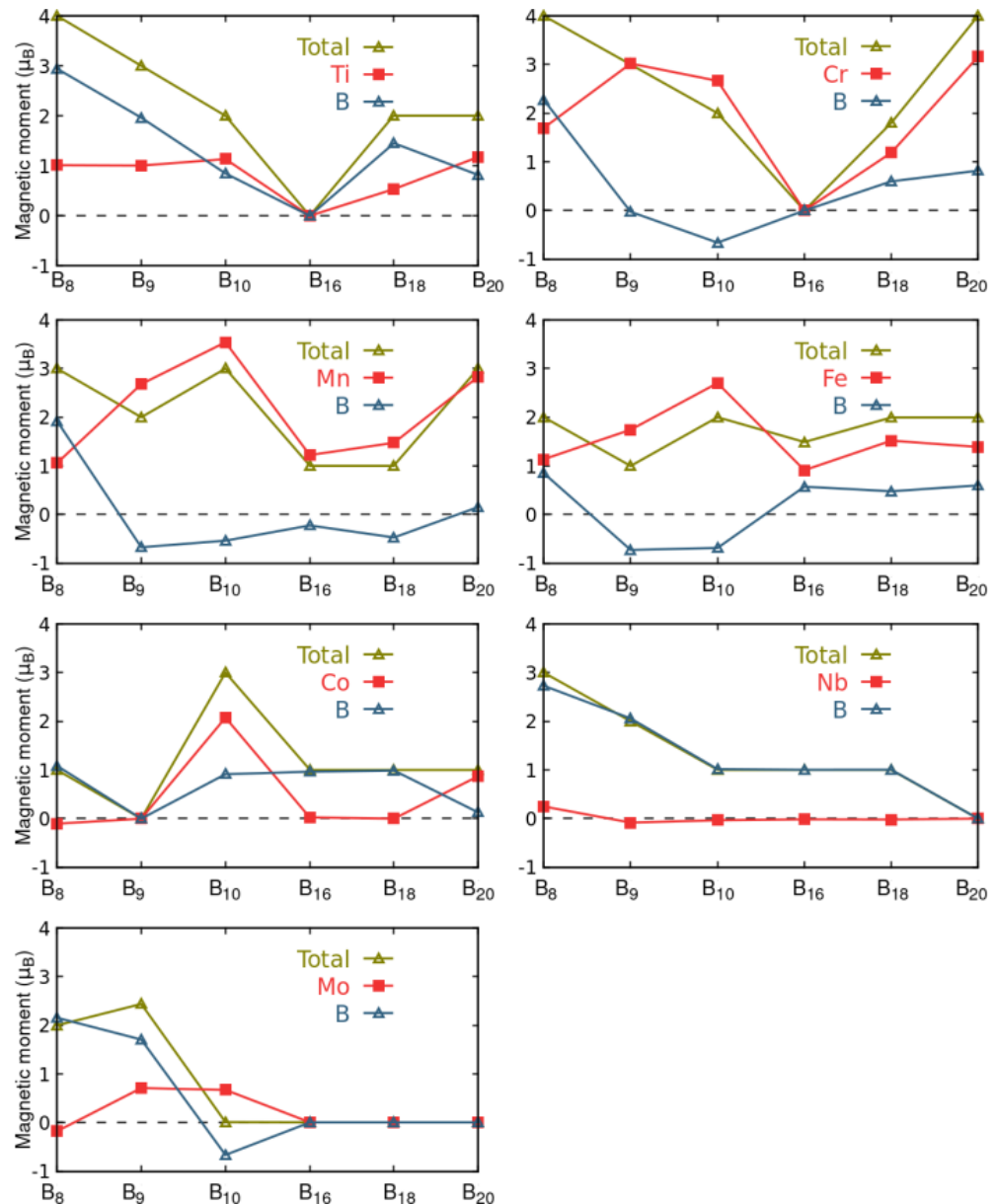
Figure 3. Total magnetic moment *m* and local magnetic moment contributions on the *y*-axis versus the cluster type in the *x*-axis. The contributions come from the TM (TM = Ti, Cr, Mn, Fe, Co, Nb, or Mn) atom and the boron atoms of each TMB$_n$ cluster. In the graph, the total magnetization is represented by yellow triangles, the magnetization due to boron atoms is represented by blue triangles, and the red squares represent the contribution from the TMs. The lines are guides for the eye.

The result presented in Figure 3 can be spatially visualized by drawing the difference between the spin-up charge density ($\rho^{\uparrow}$) and the spin-down charge density ($\rho^{\downarrow}$):

$$spin\ polarization\ density = \rho^{\uparrow}(\vec{r}) - \rho^{\downarrow}(\vec{r}).$$

This can be seen in Figure 4 where the positive and negative values of the spin polarization density are represented with yellow and cyan, respectively. This figure clearly shows that the boron atoms in all clusters become polarized, and this polarization significantly influences the total value of m. Our Löwdin population analysis provided in Section SIII of SM quantitatively demonstrates this. This analysis evidenced, in most cases, a charge transfer from/to the TM atom, which gives rise to polarization effects on the boron atoms that, as a result, contribute to the total m. The results suggest that the polarization of boron atoms is important in modulating the electron distribution, which may affect the cluster's reactivity and interactions in different environments.
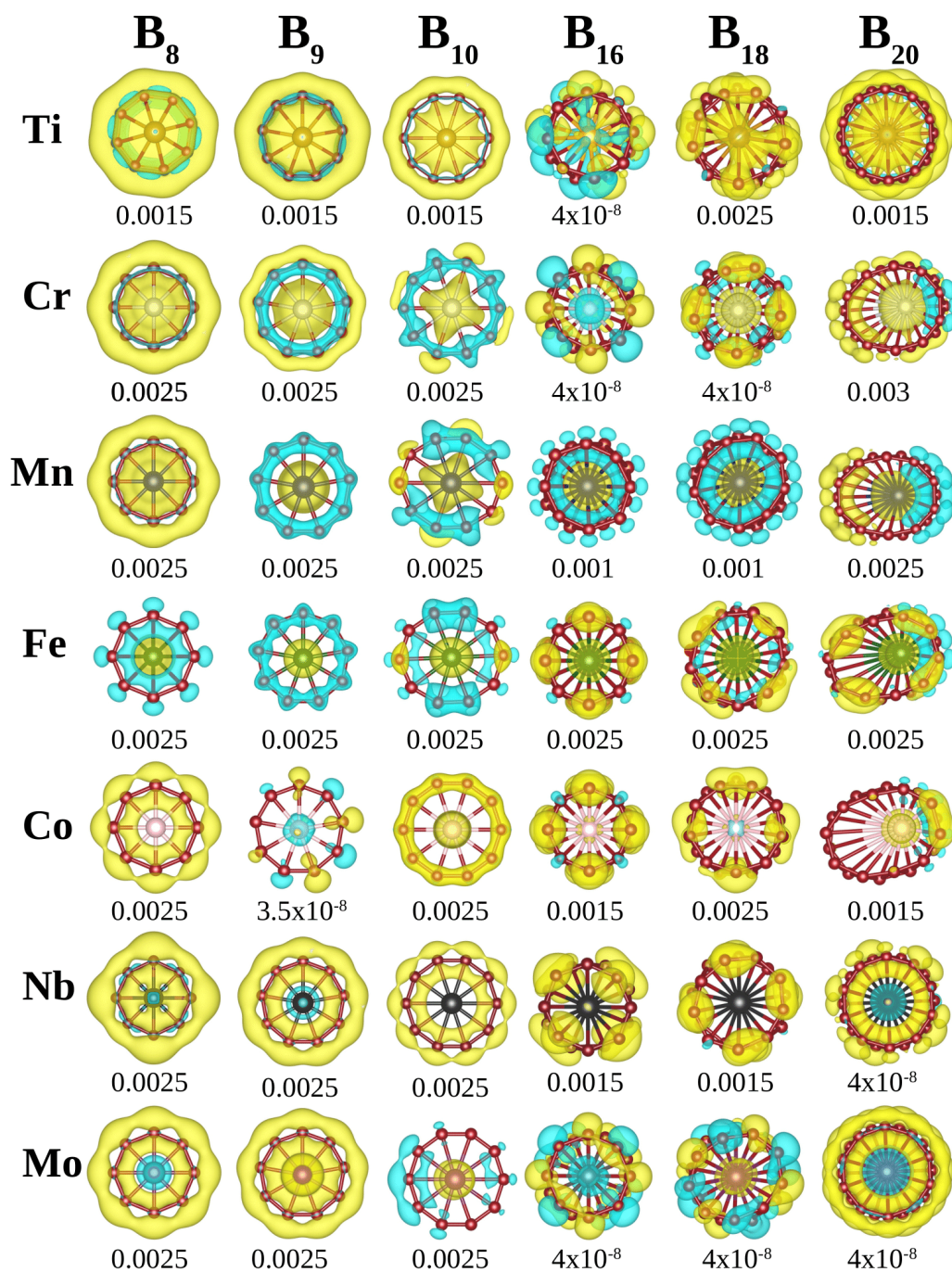
Figure 4. Difference between the spin-up charge density and the spin-down charge density. Positive and negative values are represented with yellow and cyan, respectively. The value of the iso-surface is given below each system.

4. Summary and Conclusions

The successful integration of TM atoms into the core of planar boron clusters B_n creates a fascinating class of borometallic molecules. In our study, we present the results of first-principles calculations aimed at examining the structural, electronic, and magnetic properties of boron rings with a TM atom in the center, TMB_n (with TM being Ti, Cr, Mn, Fe, Co, Nb, or Mo, and n being 8, 9, or 10), as well as boron double-rings sandwiching the metal atom, TMB_{2n}. In these molecular structures, each B atom in the circumference provides two electrons to the B–B peripheral covalent bonds and one electron to the delocalized B–TM bonds. Consequently, a TM atom with the appropriate number of valence electrons can be accommodated in the center of the boron wheel to form the TMB_n clusters, resulting in a structurally and dynamically stable borometallic cluster compound. Most of the studied clusters also possess relatively high H-L energy gaps, which may suggest low chemical reactivity. Our investigation also indicates that the overall magnetic moment of the clusters is a combination of the magnetic moment of the central TM atom and the induced magnetic moment of the peripheral boron atoms. These molecular-based magnets provide a platform for studying magnetism in the zero-dimensional limit. Furthermore, the TMB_{2n} clusters can be building blocks for one-dimensional tubular forms.

References

1. Stone, F.G.A. Chemical reactivity of the boron hydrides and related compounds. In *Advances in Inorganic Chemistry and Radiochemistry*; Elsevier: Amsterdam, The Netherlands, 1960; Volume 2, pp. 279–313.

2. Feng, B.; Zhang, J.; Zhong, Q.; Li, W.; Li, S.; Li, H.; Cheng, P.; Meng, S.; Chen, L.; Wu, K. Experimental realization of two-dimensional boron sheets. *Nat. Chem.* **2016**, *8*, 563–568. [CrossRef] [PubMed]

3. Tarkowski, T.; Gonzalez Szwacki, N.; Marchwiany, M. Structure of porous two-dimensional boron crystals. *Phys. Rev. B* **2021**, *104*, 195423. [CrossRef]

4. Tarkowski, T.; Gonzalez Szwacki, N. Boron nanotube structure explored by evolutionary computations. *Crystals* **2022**, *13*, 19. [CrossRef]

5. Tarkowski, T.; Gonzalez Szwacki, N. The structure of thin boron nanowires predicted using evolutionary computations. *Solid State Sci.* **2023**, *142*, 107241. [CrossRef]

6. Li, W.; Wu, K.; Chen, L. Epitaxial growth of borophene on substrates. *Prog. Surf. Sci.* **2023**, *98*, 100704. [CrossRef]

7. Van Duong, L.; Mai, D.T.T.; Pham-Ho, M.P.; Nguyen, M.T. A theoretical approach to the role of different types of electrons in planar elongated boron clusters. *Phys. Chem. Chem. Phys.* **2019**, *21*, 13030–13039. [CrossRef] [PubMed]

8. Pham, H.T.; Muya, J.T.; Buendia, F.; Ceulemans, A.; Nguyen, M.T. Formation of the quasiplanar B 50 boron cluster: Topological path from B 10 and disk aromaticity. *Phys. Chem. Chem. Phys.* **2019**, *21*, 7039–7044. [CrossRef] [PubMed]

9. Dong, X.; Jalife, S.; Vásquez-Espinal, A.; Ravell, E.; Pan, S.; Cabellos, J.L.; Liang, W.y.; Cui, Z.h.; Merino, G. Li2B12 and Li3B12: Prediction of the Smallest Tubular and Cage-like Boron Structures. *Angew. Chem. Int. Ed.* **2018**, *57*, 4627–4631. [CrossRef] [PubMed]

10. Van Duong, L.; Pham, H.T.; Tam, N.M.; Nguyen, M.T. A particle on a hollow cylinder: The triple ring tubular cluster B 27+. *Phys. Chem. Chem. Phys.* **2014**, *16*, 19470–19478. [CrossRef]

11. Chen, Q.; Zhang, S.; Bai, H.; Tian, W.; Gao, T.; Li, H.; Miao, C.; Mu, Y.; Lu, H.; Zhai, H.; et al. Cage-Like B41+ and B422+: New Chiral Members of the Borospherene Family. *Angew. Chem. Int. Ed.* **2015**, *54*, 8160–8164. [CrossRef]

12. Tai, T.B.; Tam, N.M.; Nguyen, M.T. Structure of boron clusters revisited, Bn with n = 14–20. *Chem. Phys. Lett.* **2012**, *530*, 71–76. [CrossRef]

13. Li, W.L.; Chen, X.; Jian, T.; Chen, T.T.; Li, J.; Wang, L.S. From planar boron clusters to borophenes and metalloborophenes. *Nat. Rev. Chem.* **2017**, *1*, 0071. [CrossRef]

14. Zhai, H.J.; Alexandrova, A.N.; Birch, K.A.; Boldyrev, A.I.; Wang, L.S. Hepta-and octacoordinate boron in molecular wheels of eight-and nine-atom boron clusters: Observation and confirmation. *Angew. Chem. Int. Ed.* **2003**, *42*, 6004–6008. [CrossRef] [PubMed]

15. Romanescu, C.; Galeev, T.R.; Li, W.L.; Boldyrev, A.I.; Wang, L.S. Aromatic metal-centered monocyclic boron rings: Co©B8- and Ru©B9-. *Angew. Chem. Int. Ed.* **2011**, *50*, 9334–9337. [CrossRef]

16. Romanescu, C.; Galeev, T.R.; Li, W.L.; Boldyrev, A.I.; Wang, L.S. Geometric and electronic factors in the rational design of transition-metal-centered boron molecular wheels. *J. Chem. Phys.* **2013**, *138*, 134315. [CrossRef]

17. Romanescu, C.; Galeev, T.R.; Li, W.L.; Boldyrev, A.I.; Wang, L.S. Transition-metal-centered monocyclic boron wheel clusters (M© B n): A new class of aromatic borometallic compounds. *Acc. Chem. Res.* **2013**, *46*, 350–358. [CrossRef] [PubMed]

18. Miao, C.; Guo, J.; Li, S. M@ B9 and M@ B10 molecular wheels containing planar nona-and deca-coordinate heavy group 11, 12, and 13 metals (M = Ag, Au, Cd, Hg, In, Tl). *Sci. China Ser. B Chem.* **2009**, *52*, 900–904. [CrossRef]

19. Pu, Z.; Ito, K.; Schleyer, P.v.R.; Li, Q.S. Planar hepta-, octa-, nona-, and decacoordinate first row d-block metals enclosed by boron rings. *Inorg. Chem.* **2009**, *48*, 10679–10686. [CrossRef] [PubMed]

20. Zhang, X.; Hu, Y.; Yuan, Y.; Li, Q.; Jiang, H.; Yang, J.; Lin, W.; Huang, H. Structure and electronic properties of neutral and anionic boron clusters doped with two tantalum atoms. *Mol. Phys.* **2022**, *120*, e2029964. [CrossRef]

21. Xu, C.; Cheng, L.; Yang, J. Double aromaticity in transition metal centered double-ring boron clusters M@B_{2n} (M = Ti, Cr, Fe, Ni, Zn; n = 6, 7, 8). *J. Chem. Phys.* **2014**, *141*, 124301. [CrossRef]

22. Yan, M.; Li, H.; Zhao, X.; Lu, X.; Mu, Y.; Lu, H.; Li, S. Fluxional Bonds in Planar B_{19}^-, Tubular Ta@B_{20}^-, and Cage-Like B_{39}^-. *J. Comput. Chem.* **2018**, *40*, 966–970. [CrossRef]

23. Ren, M.; Jin, S.; Wei, D.; Jin, Y.; Tian, Y.; Lu, C.; Gutsev, G.L. NbB_{12}^-: A new member of half-sandwich type doped boron clusters with high stability. *Phys. Chem. Chem. Phys.* **2019**, *21*, 21746–21752. [CrossRef]

24. Chen, B.; He, K.; Dai, W.; Gutsev, G.L.; Lu, C. Geometric and electronic diversity of metal doped boron clusters. *J. Phys. Condens. Matter* **2023**, *35*, 183002. [CrossRef] [PubMed]

25. Liu, X.b.; Tiznado, W.; Cui, L.J.; Barroso, J.; Leyva-Parra, L.; Miao, L.h.; Zhang, H.y.; Pan, S.; Merino, G.; Cui, Z.h. Exploring the Use of "Honorary Transition Metals" To Push the Boundaries of Planar Hypercoordinate Alkaline-Earth Metals. *J. Am. Chem. Soc.* **2024**, *146*, 16689–16697. [CrossRef]

26. Choi, D.J.; Lorente, N.; Wiebe, J.; Von Bergmann, K.; Otte, A.F.; Heinrich, A.J. Colloquium: Atomic spin chains on surfaces. *Rev. Mod. Phys.* **2019**, *91*, 041001. [CrossRef]

27. Wang, J.H.; Li, Z.Y.; Yamashita, M.; Bu, X.H. Recent progress on cyano-bridged transition-metal-based single-molecule magnets and single-chain magnets. *Coord. Chem. Rev.* **2021**, *428*, 213617. [CrossRef]

28. Ferstl, P.; Hammer, L.; Sobel, C.; Gubo, M.; Heinz, K.; Schneider, M.A.; Mittendorfer, F.; Redinger, J. Self-organized growth, structure, and magnetism of monatomic transition-metal oxide chains. *Phys. Rev. Lett.* **2016**, *117*, 046101. [CrossRef] [PubMed]

29. Jian, T.; Li, W.L.; Popov, I.A.; Lopez, G.V.; Chen, X.; Boldyrev, A.I.; Li, J.; Wang, L.S. Manganese-centered tubular boron cluster–MnB16-: A new class of transition-metal molecules. *J. Chem. Phys.* **2016**, *144*, 154310. [CrossRef] [PubMed]

30. Popov, I.A.; Jian, T.; Lopez, G.V.; Boldyrev, A.I.; Wang, L.S. Cobalt-centred boron molecular drums with the highest coordination number in the CoB16- cluster. *Nat. Commun.* **2015**, *6*, 8654. [CrossRef] [PubMed]

31. Jian, T.; Li, W.L.; Chen, X.; Chen, T.T.; Lopez, G.V.; Li, J.; Wang, L.S. Competition between drum and quasiplanar structures in RhB 18-: motifs for metallo-boronanotubes and metallo-borophenes. *Chem. Sci.* **2016**, *7*, 7020–7027. [CrossRef]

32. Li, W.L.; Jian, T.; Chen, X.; Li, H.R.; Chen, T.T.; Luo, X.M.; Li, S.D.; Li, J.; Wang, L.S. Observation of a metal-centered B 2-Ta@ B 18-tubular molecular rotor and a perfect Ta@ B 20- boron drum with the record coordination number of twenty. *Chem. Commun.* **2017**, *53*, 1587–1590. [CrossRef] [PubMed]

33. MinháTam, N.; TanáPham, H.; VanáDuong, L.; PhuongáPham-Ho, M.; ThoáNguyen, M. Fullerene-like boron clusters stabilized by an endohedrally doped iron atom: B n Fe with n= 14, 16, 18 and 20. *Phys. Chem. Chem. Phys.* **2015**, *17*, 3000–3003.

34. Wang, J.; Zhang, N.X.; Wang, C.Z.; Wu, Q.Y.; Lan, J.H.; Chai, Z.F.; Nie, C.M.; Shi, W.Q. Theoretical probing of twenty-coordinate actinide-centered boron molecular drums. *Phys. Chem. Chem. Phys.* **2021**, *23*, 26967–26973. [CrossRef]

35. Fan, Y.W.; Zhang, W.; Ge, N.N.; Li, Z. Design of Lanthanide Single-Chain Magnets Based on Tubular Segment Clusters. *J. Phys. Chem. C* **2022**, *127*, 621–626. [CrossRef]

36. Giannozzi, P.; Baroni, S.; Bonini, N.; Calandra, M.; Car, R.; Cavazzoni, C.; Ceresoli, D.; Chiarotti, G.L.; Cococcioni, M.; Dabo, I.; et al. QUANTUM ESPRESSO: A modular and open-source software project for quantum simulations of materials. *J. Phys. Condens. Matter* **2009**, *21*, 395502. [CrossRef]

37. Perdew, J.P.; Burke, K.; Ernzerhof, M. Generalized gradient approximation made simple. *Phys. Rev. Lett.* **1996**, *77*, 3865. [CrossRef]

38. Zubarev, D.Y.; Boldyrev, A.I. Comprehensive analysis of chemical bonding in boron clusters. *J. Comput. Chem.* **2006**, *28*, 251–268. [CrossRef]

39. Curtarolo, S.; Setyawan, W.; Hart, G.L.; Jahnatek, M.; Chepulskii, R.V.; Taylor, R.H.; Wang, S.; Xue, J.; Yang, K.; Levy, O.; et al. AFLOW: An automatic framework for high-throughput materials discovery. *Comput. Mater. Sci.* **2012**, *58*, 218–226. [CrossRef]

40. Li, W.L.; Ivanov, A.S.; Federič, J.; Romanescu, C.; Černušák, I.; Boldyrev, A.I.; Wang, L.S. On the way to the highest coordination number in the planar metal-centred aromatic Ta©B10- cluster: Evolution of the structures of TaB(n)- (n = 3–8). *J. Chem. Phys.* **2013**, *139*, 104312. [CrossRef]

41. Bystrom, K.; Falletta, S.; Kozinsky, B. Training Machine-Learned Density Functionals on Band Gaps. *J. Chem. Theory Comput.* **2024**, *20*, 7516–7532. [CrossRef] [PubMed]

42. Hoffmann, R.; Schleyer, P.v.R.; Schaefer, H.F. Predicting Molecules—More Realism, Please! *Angew. Chem. Int. Ed.* **2008**, *47*, 7164–7167. [CrossRef] [PubMed]